Time-resolved photoluminescence decay characteristics of bovine serum albumin-conjugated semiconductor nanocrystallites

D. Mohanta [a]; S. S. Narayanan [b]; S. K. Pal [b]; A. K. Raychaudhuri [b]

[a] Nanoscience Laboratory, Department of Physics, Tezpur University, Tezpur 784 028, Assam, India [b] S.N. Bose National Centre for Basic Sciences, Salt Lake, Kolkata 700 098, West Bengal, India

Online Publication Date: 01 June 2009

PLEASE SCROLL DOWN FOR ARTICLE

Time-resolved photoluminescence decay characteristics of bovine serum albumin-conjugated semiconductor nanocrystallites

D. Mohanta[a]*, S.S. Narayanan[b], S.K. Pal[b] and A.K. Raychaudhuri[b]

[a]*Nanoscience Laboratory, Department of Physics, Tezpur University, Tezpur 784 028, Assam, India;* [b]*S.N. Bose National Centre for Basic Sciences, Salt Lake, Kolkata 700 098, West Bengal, India*

We report processing and luminescence decay characteristics of $Cd_{1-x}Zn_xS$ composite nanocrystals (NCs) conjugated with bovine serum albumin (BSA) proteins. Time-resolved study on unconjugate NCs (with dimensions less than the bulk exciton Bohr radius) suggests that in the radiative emission, the fast (τ_1) and the slow (τ_2) carrier components are equally competitive for a given stoichiometry. Conversely, bioconjugate NCs advocate that the decay component due to the free exciton recombination is ∼9 times faster than the component due to the surface recombination emission. The observation of two distinct decay parameters is due to the fact that the NCs have experienced photostability by way of binding and protecting NC surface with biomolecules (BSA) as binding agents. The occurrence of two decay constants would help in extracting information with regard to the nature of surface recombination, free-exciton relaxation along with the strength of emission. Furthermore, with the increase in % Zn, slow carrier component gets slower owing to the incorporation of extra surface traps due to Zn/Cd incompatibility while making perfect lattice sites in the NCs. As a result, surface emission intensity gets improved compared to the radiative intensity due to core-state direct transitions. Understanding photoluminescence decay of bioconjugated NCs, on a comparative basis, would find scope for biomolecular labelling, sensing and electrophysiology applications.

Keywords: time resolved; nanocrystals; bioconjugation

1. Introduction

The bioconjugated-nanoparticles provide important schemes in nanobiotechnology as they are potential candidates for bioactive fluorescent probes in sensing, imaging, immunoassay and other similar diagnostics applications [1–6]. An alternative to conventional organic fluorophores (fluorescent dyes), luminescent nanocrystals (NCs) offer many advantages, e.g. enhanced photostability, narrow and symmetric emission spectra without red-tailing, large Stoke's shift etc., apart from the fact that they can be excited at any wavelength shorter than the wavelength of fluorescence [1,2,7]. In the recent past, the role of

*Corresponding author. Email: best@tezu.ernet.in

biomolecules was realised in nanostructure patterning and nanoscaled building blocks [8–10]. Previously, it was demonstrated that the core-shell CdSe/ZnS quantum dots can be used as fluorescent labels while conjugated to transferrin, immunoglobulin (IgG) and bovine serum albumin (BSA) [11]. Also, it was reported that the quantum dots are ideal fluorophores for multiplexed optical encoding of polymeric microbeads [12,13]. In fact, BSA (Mol. Wt $\sim$67 kD, hydrodynamic radius $\sim$7.6 nm) is a well-known protein whose molecular structure and property are known to the research community in great detail. The bioconjugated nanostructures are reported to exhibit fluorescence resonance energy transfer (FRET) owing to adequate spectral overlap between donor emission and acceptor absorption [14,15]. Following a supercritical fluid processing technique for biofunction-alisation, it was recently shown that the BSA species remain conjugated with CdS NCs over time and the conjugated nanoparticles do not agglomerate via protein–protein inter-actions [16]. Whether it is biological imaging/labelling, or application in single molecule spectroscopy, life-time aspect of luminescence patterns provides in-depth knowledge of the radiation process occurring in a given material system. The radiative intensity depends on the number of e–h recombination events, and how fast a recombination event occurs is decided by how good the surface of the nanocrystal is protected from the environment. In other words, surface defects, imperfections arising from the surface non-stoichiometry and unsaturated bonds, etc which obstruct the radiative processes, must be sealed.

In this paper, we report bioconjugation of composite $Cd_{1-x}Zn_xS$-NCs (with $x = 0, 0.5$ and 0.75) and discuss their radiative features by analysing spectroscopic data. Our time-resolved photoluminescence studies show that there exist two distinct radiative paths for bioconjugate NCs, compared to unconjugate ones both having competitive radiative emissions, due to free exciton relaxation and transition via surface traps. The nature of radiative process is discussed with regard to the stoichiometric variation and BSA conjugation.

2. Experimental: materials and methods

The fabrication procedure of NCs-BSA conjugates involves three successive steps. First, surfactant-based NCs formation in reverse micellar (RM) cages, thiol-stabilisation for making NCs surface hydrophilic and finally, NCs entanglement with BSA. In the first step, we have followed the RM route described by Cizeron and Pileni [17]. The degree of hydration $w_0 = [H_2O]/[AOT] = 8.9$ was kept constant so that one can obtain definite hydrodynamic size (dia) of the reverse micelles (i.e., $d \sim 4w_0 = 3.6$ nm) and thus capable of accommodating NCs of a few atomic clusters only [18,19].

About 440 mg of surfactant bis(2-ethylhexyl) sulfosuccinate (aerosol-OT, AOT, Aldrich & Co.) was dissolved in 16.2 mL of *n*-heptane followed by dropwise addition of 54 μL de-oxygenated water under vigorous stirring. The mixture was stirred for about 3 h until a homogeneous microemulsion was obtained. The resulting precursor was divided into two equal parts A and B. Part A was used for the synthesis of CdS while part B was meant for the synthesis of $Cd_{0.50}Zn_{0.50}S$.

Next, part A was sub-divided into two equal parts A$^{/}$ and A$^{//}$. Then, (7 μL, 1 M) Cd^{2+} solution was added to A$^{/}$ so as to receive an optically homogeneous solution. Similarly, (1.5 μL, 1 M) Na_2S was transferred to A$^{//}$ by means of a syringe. For complete nucleation of CdS NCs, A$^{/}$ and A$^{//}$ were then mixed at once and stirring ($\sim$200 rpm) was continued

for 10–12 h in a dark chamber. On the other hand, precursor B was sub-divided into part B' (4.1 mL), B'' (2 mL) and B''' (2 mL). Then (7 μL, 1 M) Cd^{2+} and (7 μL, 1 M) Zn^{2+} solutions were added to B'' and B''', whereas (26 μL, 1 M) S^{2-} solution was transferred to B'. As-received mixtures B'' (containing Cd^{2+}) and B''' (containing Zn^{2+}) were added at once under stirring environment. Finally, B' (containing S^{2-}) was injected drop-wise and the sample was kept under stirring overnight for perfect nucleation of the desired $Cd_{0.50}Zn_{0.50}S$ NCs. In a similar way, $Cd_{0.25}Zn_{0.75}S$ NCs were synthesised by choosing appropriate volumetric concentration of Zn^{2+} and Cd^{2+} while mixed with S^{-2}. Note that as the microreactors containing Zn^{2+} and Cd^{2+} (with $[Cd^{2+}] + [Zn^{2+}]/[S^{2-}] = 1$) were continuously in a state of dynamic equilibrium, the favourable possibility of obtaining composite system ($Cd_{1-x}Zn_xS$) was more compared to the existence of independent CdS and ZnS phases. A typical synthesis route of CdS and CdZnS NCs is shown in the flow chart diagram (Figure 1(a)).

In the second step, for thiol solubilisation, 1 mL of given NC sample was transferred carefully to a 5 mL volumetric flask. Methanol (1 mL) was added dropwise till complete precipitation. The wet precipitate was wobbled well. In another centrifuge, 0.1 mL of mercaptoacetic acid (thioglycolic acid, Loba Chemi) was taken and transferred to a 10 mL volumetric flask containing 1 mL of dimethylformamide (DMF). Subsequently, the NC precursor was added and the whole mixture was vortexed and sonicated for about 45 min. The clear and transparent solutions containing thiol-stabilised NCs were stored for 1–2 days prior to bioconjugation.

Chemically reduced BSA (99.9% pure, Sigma-Aldrich & Co.) was prepared by denaturing BSA in 1 mM sodium borodydride in water at ~70°C. Excess borohydride was removed by spontaneous decomposition by heating. For effective bioconjugation, (2.6 mL, 197 μM) BSA was treated with (0.4 mL, 25 μM) NCs. After labelling, the test tubes were shaken well and made airtight with teflon. The samples were incubated for 3–5 days at (65–70°C). At last the samples were centrifuged (~12,000 rpm) for ~5 h followed by decantation. The decant was the actual NCs-BSA conjugate specimen, stored for subsequent experimentation. Thiol-treated CdS-NCs including BSA conjugation steps are shown in the block diagram (Figure 1(b)).

The samples were analysed by optical absorption spectroscopy (OAS), steady-state photoluminescence (PL) spectroscopy and time-resolved photoluminescence (TR-PL) spectroscopy, respectively. Note that a typical BSA molecule (containing two tryptophans) absorbs light at ~278 nm, but emits within 310–348 nm, depending on the excitation wavelength of light [13]. In order to isolate NC emission from tryptophans, we had selected $\lambda_{ex} = 375$ nm line of excitation, and corresponding emission at ~430 nm was analysed by a standard picosecond-resolved time correlated single photon counting (TCSPC) system. The commercially available setup was a picosecond diode laser pumped time-resolved fluorescence spectrophotometer (LifeSpec-ps, Edinburgh Instrument, UK).

3. Results and discussion

Figure 2 represents a set of optical absorption spectra of the synthesised NCs samples. The absorption edge (λ_e) is the intersection of the sharply decreasing region of the spectrum with the baseline, correlated to the particle size by expression
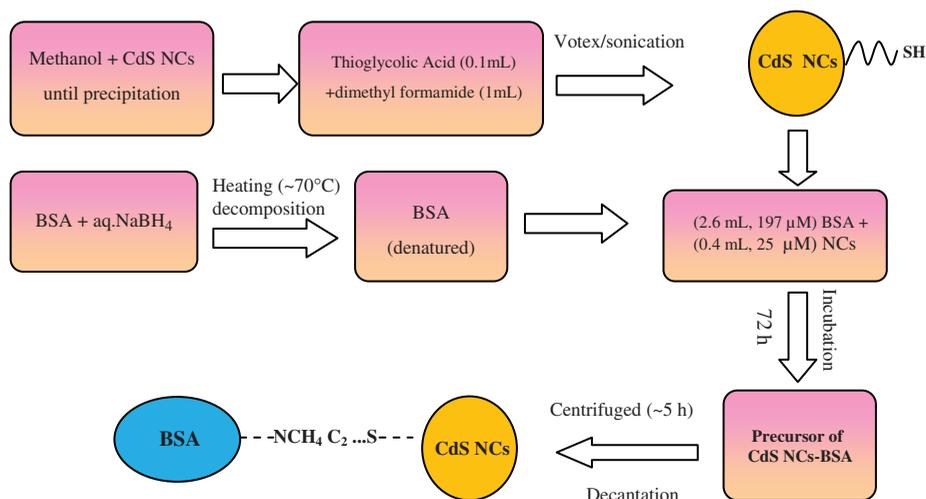
(a)
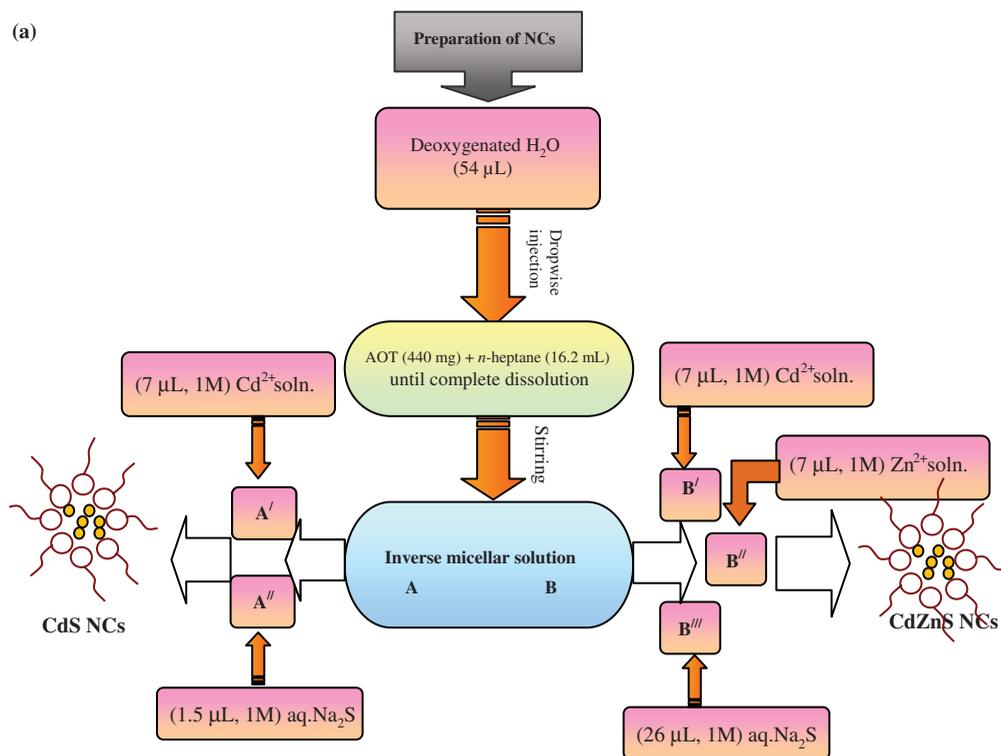
(b)

Figure 1. A typical flow chart diagram for obtaining (a) unconjugate CdS- and CdZnS-NCs and (b) thiol-capped and BSA-conjugated CdS NCs.
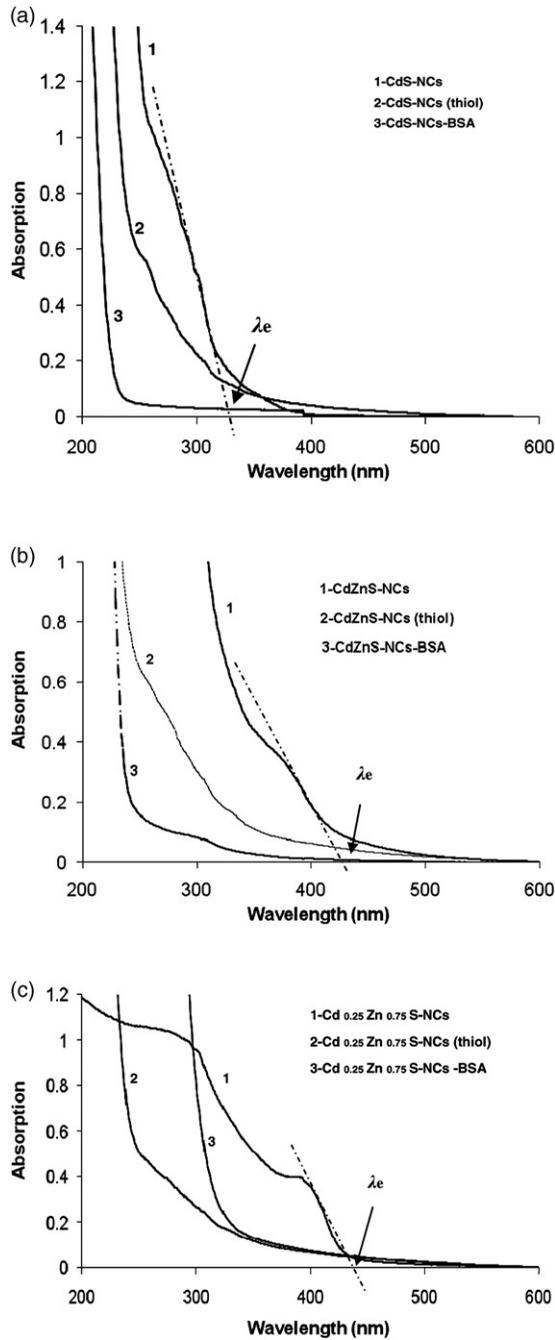
Figure 2. Optical absorption spectra (OAS) of (a) CdS, (b) CdZnS and (c) $Cd_{0.25}Zn_{0.75}S$-NCs systems. Numbers (1), (2) and (3) represent untreated, thiol-stabilised and BSA-NCs conjugates, respectively.
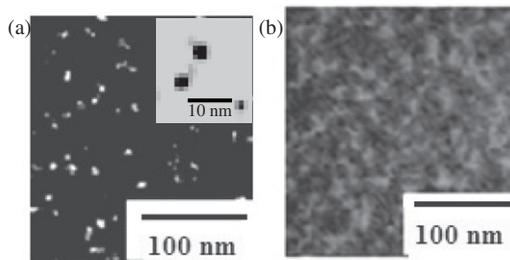
Figure 3. High resolution electron microscopy images of (a) CdS-NCs and (b) CdS-BSA conjugates. A magnified view of isolated, spherical CdS-NCs (~2 nm) is shown in the figure inset – (a).

[20,21]: $2r = 1/(0.1338 - 0.0002345 \lambda_e)$. We have estimated the absorption onsets for CdS, CdZnS and $Cd_{0.25}Zn_{0.75}S$ NCs as 340, 425 and 440 nm, respectively (Figure 2(a1)–(c1)). Accordingly, NCs (within strong confinement regime ($r < a_B$, Bohr radius)) were obtained with average sizes calculated as 1.8, 2.9 and 3.3 nm. The size of CdS NCs was verified by transmission electron microscopy (TEM), and is shown in Figure 3. The unconjugate CdS NCs sample displays isolated particles (~2 nm) with very narrow size distribution (Figure 3(a)). Bovine serum albumin-conjugated NC structures are shown in Figure 3(b). Note that the synthesis steps involved definite NCs concentration, and the microscopic imaging was done at similar magnifications. Statistical analysis on various micrographs has helped us in calculating bioconjugation conversion efficiency i.e., ~78%. Since a number of biomolecules are attached to individual nanoparticles, clustering effect was seen in Figure 3(b), compared to Figure 3(a).

It is worth mentioning here that in case of a bulk, depending on the Cd/Zn stoichiometry, the optical band gap of a CdZnS composite will correspond to a value in between energy gaps of CdS ($E_g = 2.4$ eV) and ZnS ($E_g = 3.7$ eV). Therefore, with the increase of Zn content there can be shifting of the absorption edge towards blue (towards higher energy). Needless to say, such a situation could also have been realised in our case, had composite NCs of exactly identical sizes been produced. Since the energy gap is extremely sensitive to the NC size particularly, when it is comparable to or smaller than the Bohr radius, the discussion on shifting of the absorption edge is beyond the scope of the present study. On the other hand, we have noticed exciton absorption features for all the cases of unconjugate NCs. Thiol-treatment and BSA-conjugation had featureless characteristics owing to the surface treatment of functionalization of NCs due to the functionalization of ligand specific binding agents (Figure 2(a2), (a3), (c2), (c3)). As bioconjugates have at least eight times more concentrated BSA molecules (which absorbs ~278 nm) with respect to NCs, absorption feature of the former had affected the excitonic feature of the later. Shown in Figure 4(a)–(c) are steady-state photoluminescence of composite $Cd_{1-x}Zn_xS$ ($x = 0, 0.5, 0.75$) NCs that reveal intense emission when they are untreated. However, the intensity of such samples was found to be suppressed with aging (not shown) and might have resulted due to the particle growth within the nanoreactors of the reverse micelles, which were in a state of dynamic Brownian motion. On the other hand, PL is suppressed significantly (11–17%) for thiol-treated and BSA-conjugated
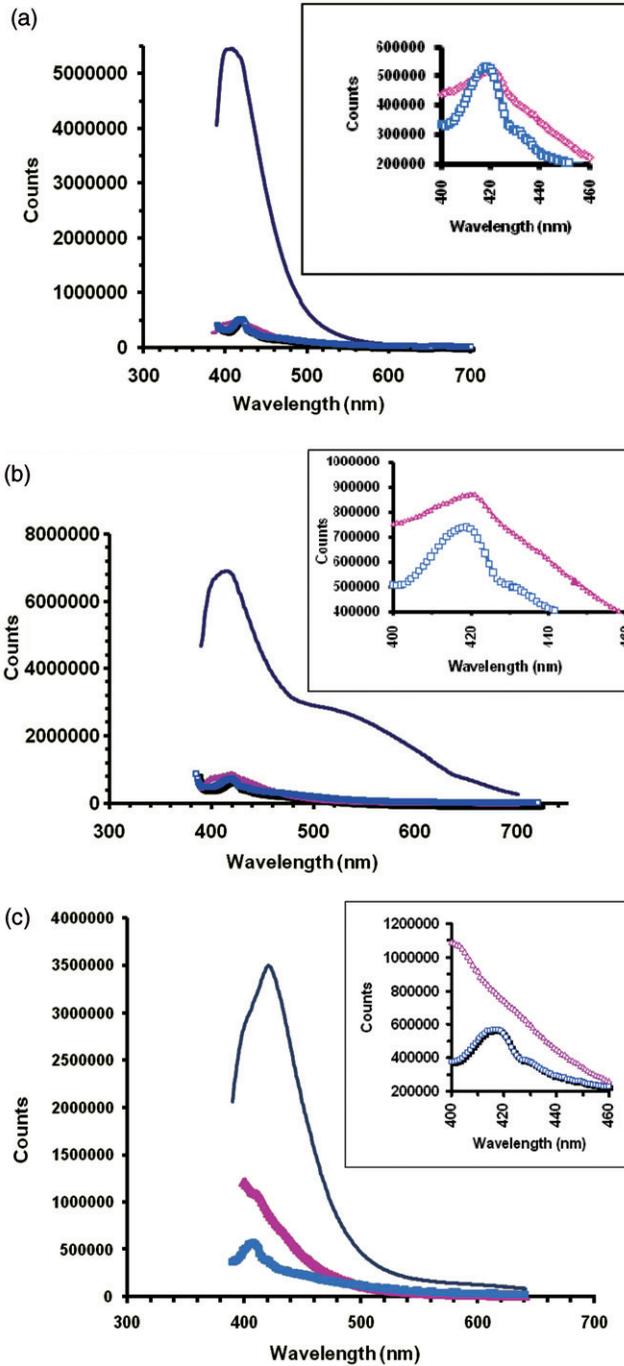
Figure 4. Steady-state PL spectra of (a) CdS, (b) CdZnS and (c) $Cd_{0.25}Zn_{0.75}S$-NCs systems. Figure insets represent spectral responses in the selective wavelength range (400–460 nm) highlighting prominent peak positions. Symbols (—), (▲) and (□) correspond to untreated, thiol-stabilised and BSA-NCs conjugates, respectively.

samples as a result of suppression of radiative emission due to adequate surface modification and reconstruction while synthesis was in progress. Nevertheless, PL intensity was found to be fairly stable with aging up to 1–2 weeks. For a given stoichiometry, the emission peak for the untreated NCs was found to be close to the bioconjugated NCs. The first prominent peak at ~410–430 nm was ascribed to the near band edge emission. A broad emission peak at ~520 nm arising due to surface deep trap states (non-radiative centers) is seen for CdZnS-NCs. The broad spectrum is owing to the unavoidable chemical incompatibility of Cd and Zn realised while forming a NCs lattice. Such a lattice mismatch is presumably minimum when either kind of atom dominates, as noticed for CdS-NCs and $Cd_{0.25}Zn_{0.75}S$ NCs cases (Figure 4(a) and (c)). Figure insets are shown to compare the emission responses of thiol-treated NCs and NCs-BSA conjugates.

In general, the PL decay curve, which has a bi-exponential form, is widely recognised for colloidal NCs and is given by [22,23]:

$$A = A_1 e^{-t/\tau_1} + A_2 e^{-t/\tau_2} \tag{1}$$

where τ_1 and τ_2 are the decay time constants of the rapid and slow processes, and A_1 and A_2 are the corresponding intensities, respectively. Again, a PL decay rate of a semiconductor includes the sum of the radiative and non-radiative decay rates [24]: $k = k_{NR} + k_R$, and knowing that the decay rates and decay time constants are inversely related [23,25], we have as

$$\tau_{PL}^{-1} = \tau_{NR}^{-1} + \tau_{R}^{-1} \tag{2}$$

where τ_{PL}, τ_R and τ_{NR} are the PL, radiative and non-radiative decay time constants, respectively. For a pure and ideal system, one can compare the fast component (τ_1) and the slow component (τ_2) with the non-radiative emission decay time (τ_{NR}) and radiative decay time (τ_R). In fact, non-radiative recombinations give rise to a fast relaxation of the excited carriers, while the slow decay term is usually due to the radiative recombination of free or localised excitons. Ideally, the fast component of a similar binary NCs system is of the order of several ps and is assigned to the luminescence quenching defects/deep trap centers [23,24,26]. On the other hand, slow component is well known and is assigned to the radiative recombination of excitons in semiconductors with life time 1 ns [23,27]. One can also calculate the radiative time using a popular equation [28]:

$$\tau_{rad} = \frac{2\pi\varepsilon_0 m_0 c^3}{n e^2 \omega^2 f} \tag{3}$$

with ε_0, m_0, e and c have their usual meanings. Here, n and ω represent the refractive index and the angular frequency (corresponding to the energy band of the material), while f being exciton oscillator strength. For CdS, considering $n = 2.33$, $\omega = 3.74 \times 10^{15}\,s^{-1}$ and $f \sim 1$ as the upper limit for bound excitons, radiative life time (τ_{rad}) is calculated to be ~1.64 ns.

Our TR-PL results have predicted time constants ~2 and 18–20 ns (Table 1). Therefore, the contribution due to deep trap centers/impuritiy states with time constant in the ~ps scale and cases like multiphonon processes can be ignored here. The results are in good agreement with the recent investigations reported by Wang and coworkers who also suggested biexponential response of the ns components [29]. It is evident that these two ns components

Table 1. PL-decay constants for various $Cd_{1-x}Zn_xS$-NCs and BSA conjugates.

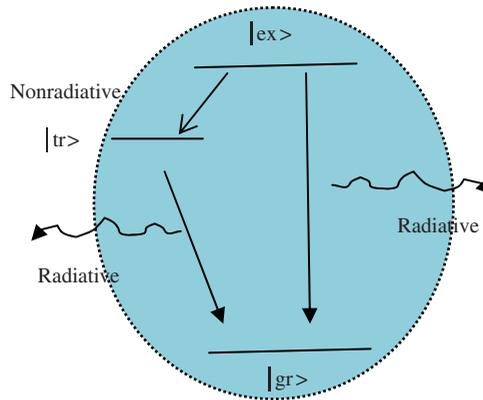| Sl.	Sample $Cd_{1-x}Zn_xS$	x (%)	τ_f (ns)	τ_s (ns)	A_f (%)	A_s (%)	τ_s/τ_f	τ (ns)
1	CdS-NCs	0	24.13	24.13	50	50	1	12.06
2	CdS-NCs-BSA		2.07	18.84	80.9	19.1	9.1	1.87
3	CdZnS-NCs	50	21.25	21.25	50	50	1	10.62
4	CdZnS-NCs-BSA		2.21	20.07	78.8	21.2	9.08	1.99
5	$Cd_{0.25}Zn_{0.75}S$-NCs	75	17.54	17.54	50	50	1	8.77
6	$Cd_{0.25}Zn_{0.75}S$-NCs-BSA		2.34	20.31	74.3	25.7	8.68	2.09

Figure 5. Schematic view of the radiative emission process in NCs.

are as a result of the two distinct radiative events. First, the shorter life time can be ascribed to the direct radiative transitions of the free excitons (core-state recombination) while the second, relatively slower component should be due to the radiative recombination via surface-trap sites. In contrast, the radiative nature of the fast process (shorter-life time) had been studied both experimentally [30] and theoretically [31], and was attributed to the initially populated core-state recombination of carriers. A schematic of radiative emission feature is shown in Figure 5, where $|gr\rangle$, $|ex\rangle$ and $|tr\rangle$ represent ground state, excited state and surface trap state, respectively. As the radiative part in Equation (2) has two components (the first, due to direct recombination emission and the slow due to surface recombination emission), we can rewrite for the radiative time constant as:

$$\tau_2^{-1} = \tau_f^{-1} + \tau_s^{-1} \tag{4}$$

with τ_f and τ_s being fast and slow components, respectively.

Again, knowing that the two ns components exhibit exponential features, which constitute the second term in Equation (2), in conjunction with Equation (4):

$$A = A_f A_s e^{-t\left(\tau_f^{-1} + \tau_s^{-1}\right)} \tag{5}$$

where $A = A_f A_s$, the combined radiative intensity. The logarithmic expression will read as:

$$\log A = \log A_f + \log A_s - t\left(\frac{\tau_f + \tau_s}{\tau_f \tau_s}\right) \tag{6}$$
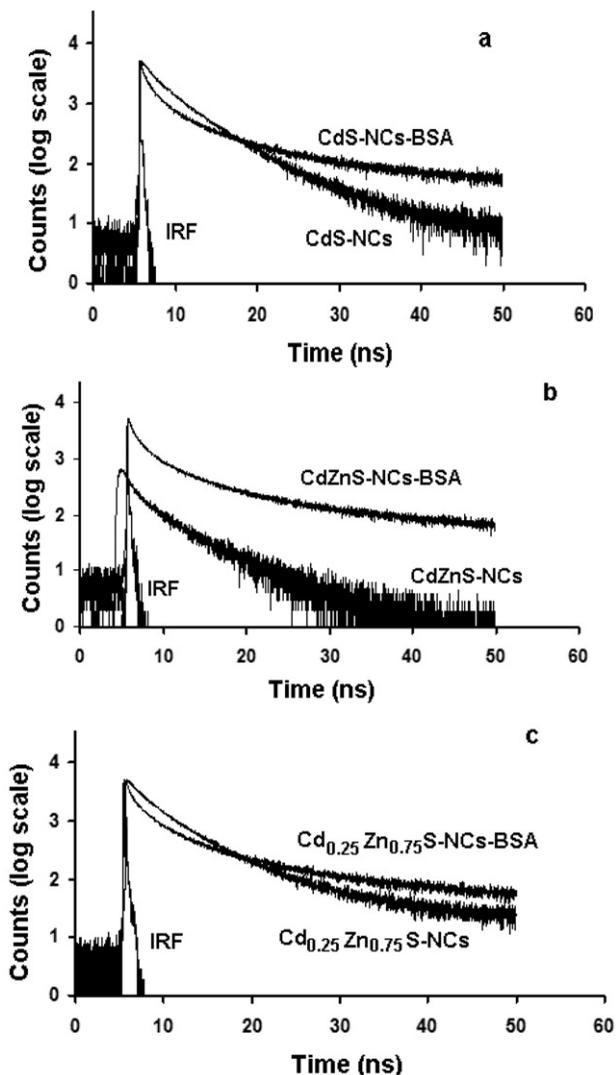
Figure 6. Time-resolved photoluminescence spectra ($\lambda_{ex} = 375$ nm; $\lambda_{em} = 430$ nm) of (a) CdS, (b) CdZnS and (c) $Cd_{0.25}Zn_{0.75}S$-NCs systems.

and for equally competitive NC core-state and surface recombinations ($\tau_f = \tau_s$, $A_f = A_s$),

$$\log A = \log A_f^2 - \frac{2t}{\tau_f} = \log A_s^2 - \frac{2t}{\tau_s} \tag{7}$$

The TR-PL responses of various NCs are shown in Figure 6(a–c) and Table 1. The NCs-BSA conjugates exhibit truly bi-exponential features with distinct fast and slow components. In contrast smooth exponential decay features were noticed for the unconjugate NCs. We notice $\tau_f = \tau_s$ for all of the untreated NC systems, but the decay

Figure 7. Decay time constant *vs*. stoichiometry (% *x*, Zn) for $Cd_{1-x}Zn_xS$-NCs and BSA conjugates.

components get reduced with stoichiometry (% *x*, Zn composition (Figure 7)) variation. Thus, one can say that the PL decay of the unconjugate NCs exhibits single exponential behavi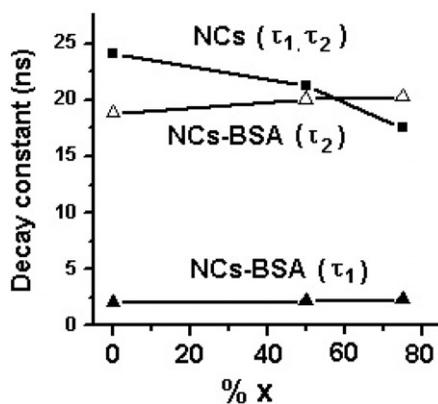our as per Equation (7), where the radiative processes due to the core-state and the surface-related emissions are equally competitive. Upon BSA conjugation, one finds distinctly different time constants, e.g. fast component $\tau_f \sim 2.07$–2.34 ns and slow component $\tau_s \sim 18.84$–20.31 ns; fairly uniform for different stoichiometry values (Figure 7). In other words, NCs bioconjugates display PL decay with radiative emission due to the free excitons about nine times faster than the carrier recombination emission via surface traps.

While both the time components are reasonably stable for NC-BSA-conjugated structures, the unconjugate NCs display significant variation in time constants (17.54–24.13 ns) with variation in stoichiometry. In the later case, the variation in time constants could have been due to the stoichiometry dependent electronic structure modification of the NCs. The electronic structure modification could be due to significant chemical incompatibility of Zn (covalent atm. rad. $\sim$0.131 nm) and Cd (covalent atm. rad. $\sim$0.148 nm) in $Cd_{1-x}Zn_xS$ which had led to lattice contractions and hence, lattice defects on the NC surface. Noting here that for a spherical NC, surface-to-volume ratio $\sim 3/r_n$, r_n being the NC radius (which actually depends on the covalently bonded atomic radius and the number of atoms therein), there can be a drastic variation in the number of surface defects when there is a variation in stoichiometry. This has affected the radiative recombination time constants at large (Table 1). Nevertheless, the most striking feature of albumin is its ability to bind reversibly an incredible variety of ligands and therefore, BSA-conjugated NCs could bring in adequate surface reconstruction and organisation of the surface atoms passivating the surface defects to a great extent. This helps in protecting NCs from photobleaching, keeping distinct radiative pathways intact and, thus, improving environmental stability. For BSA-NCs, the rapid and slow components are estimated to be $\sim$2 and $\sim$18–20 ns, respectively (Table 1, Figure 7). One can say that unconjugated NCs suffer from unwanted photobleaching, whose luminescence decay patterns are affected by alloying (%*x*) whereas bioconjugated BSA-NCs exhibit rather stable and distinct radiative patterns, independent of stoichiometry while the NCs are close to the strong confinement regime. In the strong confinement regime, electron and hole

confine independently in the NCs. Now, since the electron has a smaller effective mass than the hole in a NC, it has a greater chance of going into the surface rather than staying inside the core of the NC [32]. On the other hand, the heavy hole can remain at the center of mass of the NC [33]. Compared to the unconjugate NCs, significant decrease in the fast component (τ_f) of BSA-NCs might be due to the suppression of screening of the radiation field inside the NCs making ease of the core-state recombination [31]. Now, since the relative intensities A_f and A_s are dependent on the number of radiative occurrences due to the free exciton relaxation and relaxation via surface states, the processes can be stoichiometry dependent. In our case, contribution (A_f) due to the core-state radiative recombination emission was found to be highest (80.9%) for CdS-NCs-BSA structures. It was, however, suppressed to 74.3% for $Cd_{0.25}Zn_{0.75}S$-BSA systems. In contrast, the surface-related radiative intensity (A_s), was 19.1 (lowest) and 25.7% (highest) for CdS-BSA and $Cd_{0.25}Zn_{0.75}S$-BSA, respectively (Table 1). Even for crystallites of fairly uniform dimension, since there can be additional surface trap states due to Cd/Zn incompatibility, the surface related contribution to the emission intensity is found to be higher in case of $Cd_{0.25}Zn_{0.75}S$-BSA system. It was believed that, owing to the surface binding capability of BSA, which is more efficient in case of CdS-BSA, the radiative intensity due to core-state recombination emission should be higher. Surface binding would be relatively weak for $Cd_{0.25}Zn_{0.75}S$-BSA systems and hence there is enhancement in surface emission intensity in comparison to CdS-BSA. The CdZnS-BSA NCs display emission intensities, which is intermediate between above discussed samples. Hence, bioconjugated samples exhibit maximum surface reconstruction for minimum chemical incompatibility and vice-versa.

On the other hand, two possibilities are invoked for the origin of non-radiative processes: (i) defect concentration changes due to the variation in Cd and Zn composition to form NCs and (ii) surface defects due to the large s/v ratio for NCs. It is expected that the non-radiative channels are due to lattice mismatch as a result of difference in atomic sizes of Zn and Cd as described above. The amount of lattice mismatch depends on the stoichiometric ratio Zn:Cd, which in turn results in strain-induced surface states. Thus, surface recombination emission is affected by such surface defects. ZnS in the bulk form is considered as a phosphorescent material capable of giving out light up to several hundred seconds while CdS is a good fluorescent candidate. A relative change in Cd to Zn stoichiometry would be very much desired while looking at physiological activities like bioimaging and sensing. For instance, in an electrophysiology experiment, the helical peptides, e.g. alamethicin [34], gramicidin [35] etc can form voltage/ligand gated ion channels across phospholipid bilayers. On the other hand, the importance of ion channel mechanism has already been experienced *in vivo* real cells. Ion channel activity due to the non-selective ion transport was reported in human red blood cell (RBC) that can explain the nature of blood clotting [36], while the importance of light sensitivity to the ion channels was realised for neuronal firing [37]. Due to the limited advantage and very often chemical reactivity of the organic fluorophors/dyes they can not be used in these experiments, especially while going for simultaneous optical and electrical measurements. Since the surface emission is highly controlled with Zn/Cd variation, one can use NCs-entangled ion channel peptides in order to understand dynamic nature of pore formation, reactivity of peptides with the bilayer in the process of making ion channels. In addition, opening and closing states of the ion channels can be related with the radiative emission that would occur in a given composite NCs, tagged to peptides. Moreover, NCs being

efficient and alternative to conventional fluorophors can open up an area of study where the peptides do not undergo voltage gated expression but display either ligand gated or mechanically gated ion channel response. Apart from the unconjugate cases, where radiative emission is equally competitive for slow and fast decay components, a large incremental % of Zn, resulted in slow decay of the surface emission with a decay time $\tau_s \sim 20.31$ ns (for a conjugated system with $Zn:Cd = 3:1$). It clearly indicates that though the surface reconstruction takes place in BSA conjugates, the contribution to the lattice mismatch cannot be ignored especially when the stoichiometry variation is very high. In addition, BSA-NCs system provides an ideal scheme where the core-state radiative emission can contribute $\sim$9 times faster than the surface trap recombination emission.

4. Summary

In summary, we have produced stable composite semiconductor NCs adopting a RM route. Upon thiol-stabilisation, BSA was conjugated independently with CdS, CdZnS and $Cd_{0.25}Zn_{0.75}$S-NCs systems. We have also addressed the light-emission process by studying steady-state and time-resolved PL measurements. We found that unconjugate NCs exhibit competitive radiative processes while bioconjugated NCs reveal that the luminescence decay proceeds through distinct paths with fast component about nine times faster than the slow component. The fast component is found to be fairly stable irrespective of stoichiometry variation. With reference to the stoichiometry variation and bioconjugation, various decay constants are estimated and discussed on a comparative basis. We believe that BSA conjugation could help in surface reconstruction, to the extent chemical incompatibility of Cd and Zn realised on the NC lattice. Hence, NC-BSA proteins are advantageous in the sense that they can protect and preserve fluorescence, especially when NCs are in the strong confinement regime. Understanding dynamics of NC surface emission pattern would provide electronic and optical transduction of the biological phenomena in many electrophysiological experiments including intracellular imaging with high selectivity and specificity.

Acknowledgements

References

[1] M. Bruchez, M. Moronne, P. Gin, S. Weiss, and A.P. Alivisatos, *Semiconductor nanocrystals as fluorescent biological labels*, Science 281 (1998), pp. 2013–2016.
[2] H. Matssoussi, J.M. Mauro, E.R. Goldman, G.P. Anderson, V.C. Sundar, F.V. Milkulec, and M.G. Bawendi, *Self-assembly of CdSe−ZnS quantum dot bioconjugates using an engineered recombinant protein*, J. Am. Chem. Soc. 122 (2000), pp. 12142–12150.
[3] J.K. Jaiswal, H. Mattoussi, J.M. Mauro, and S.M. Simon, *Long-term multiple color imaging of live cells using quantum dot bioconjugates*, Nat. Biotechnol. 21 (2003), pp. 47–51.
[4] I.L. Medintz, H.T. Uyeda, E.R. Goldman, and H. Mattoussi, *Quantum dot bioconjugates for imaging, labelling and sensing*, Nat. Mater. 4 (2005), pp. 435–446.

[5] E.R. Goldman, I.L. Medintz, J.L. Whitley, A. Hayhurst, A.R. Clapp, H.T. Uyeda, J.R. Deschamps, M.E. Lassman, and H. Mattoussi, *A hybrid quantum dot−antibody fragment fluorescence resonance energy transfer-based TNT Sensor*, J. Am. Chem. Soc. 127 (2005), pp. 6744–6751.

[6] C.-Y. Zhang, H.-C. Yeh, M.T. Kuroki, and T.-H. Wang, *Single-quantum-dot-based DNA nanosensor*, Nat. Mater. 4 (2005), pp. 826–831.

[7] F. Wang, W.B. Tan, Y. Zhang, X. Fan, and M. Wang, *Luminescent nanomaterials for biological labeling*, Nanotechnology 17 (2006), pp. R1–R13.

[8] W.J. Parak, D. Gerion, T. Pellegrino, D. Zanchet, C. Micheel, S.C. Williams, R. Boudreau, M.A. Le Gros, C.A. Larabell, and A.P. Alivisatos, *Biological applications of colloidal nanocrystals*, Nanotechnology 14 (2003), pp. R15–R27.

[9] P.S. Weiss, *Nanotechnology: molecules join the assembly line*, Nature 413 (2001), p. 585.

[10] T. Yokoyama, S. Yokoyama, T. Kamikado, Y. Okuno, and S. Mashiko, *Selective assembly on a surface of supramolecular aggregates with controlled size and shape*, Nature 413 (2001), pp. 619–621.

[11] W.C. Chan and S. Nie, *Quantum dot bioconjugates for ultrasensitive nonisotopic detection*, Science 281 (1998), pp. 2016–2018.

[12] M. Han, X. Gao, J.Z. Su, and S. Nie, *Quantum-dot-tagged microbeads for multiplexed optical coding of biomolecules*, Nat. Biotechnol. 19 (2001), pp. 631–635.

[13] X. Gao, W.C.W. Chan, and S. Nie, *Quantum-dot nanocrystals for ultrasensitive biological labeling and multicolor optical encoding*, J. Biomed. Optics 7 (2002), pp. 532–537.

[14] N.N. Mamedova, N.A. Kotov, A.L. Rogach, and J. Studer, *Albumin−CdTe nanoparticle bioconjugates: preparation, structure, and interunit energy transfer with antenna Effect*, Nano Lett. 1 (2001), pp. 281–286.

[15] S. Wang, N.N. Mamedova, N.A. Kotov, W. Chen, and J. Studer, *Antigen/Antibody immunocomplex from CdTe nanoparticle bioconjugates*, Nano Lett. 2 (2002), pp. 817–822.

[16] M.J. Meziani, P. Pathak, B.A. Harruff, R. Hurezeanu, and Y.-P. Sun, *Direct conjugation of semiconductor nanoparticles with proteins*, Langmuir 21 (2005), pp. 2008–2011.

[17] J. Cizeron and M.P. Pileni, *Solid Solution of $Cd_yZn_{1−y}S$ nanosize particles made in reverse micelles*, J. Phys. Chem. 99 (1995), pp. 17410–17416.

[18] P.L. Luisi, M. Giomini, M.P. Pileni, and B.H. Robinson, *Reverse micelles as hosts for proteins and small molecules*, Biochim. Biophys. Acta 947 (1988), pp. 209–246.

[19] P. Majumder, R. Sarkar, A.K. Shaw, A. Chakraborty, and S.K. Pal, *Ultrafast dynamics in a nanocage of enzymes: solvation and fluorescence resonance energy transfer in reverse micelles*, J. Coll. and Interf. Sci. 290 (2005), pp. 462–474.

[20] L. Spanhel, M. Hasse, H. Weller, and A. Henglein, *Photochemistry of colloidal semiconductors: surface modification and stability of strong luminescing CdS particles*, J. Am. Chem. Soc. 109 (1987), pp. 5649–5655.

[21] M. Moffitt and A. Eisenberg, *Size control of nanoparticles in semiconductor-polymer composites: control via multiplet aggregation numbers in styrene-based random ionomers*, Chem. Mater. 7 (1997), pp. 1478–1184.

[22] L.Y. GaO, Y.-J. Lu, J.S. Zheng, Z.-G. Cai, H.-Y. Sang, and X.-R. Zeng, *Time-resolved photoluminescence study of $Ga_{0.52}In_{0.48}P$ alloys*, Euro. Phys. J. B 28 (2002), pp. 145–148.

[23] C.P. Li, L. Guo, Z.Y. Wu, L.R. Ren, X.C. Ai, J.P. Zhang, Y.Z. Lv, H.B. Xu, and D.P. Yu, *Photoluminescence and time-resolved photoluminescence of star-shaped ZnO nanostructures*, Solid State Commun. 139 (2006), pp. 355–359.

[24] G. Schlegel, J. Bohnenberger, I. Potapova, and A. Mews, *Fluorescence decay time of single semiconductor nanocrystals*, Phys. Rev. Lett. 88 (2002), pp. 137401-1–137401-4.

[25] S. Hong, T. Joo, W. Park, Y.H. Jun, and G.-C. Yia, *Time-resolved photoluminescence of the size-controlled ZnO nanorods*, Appl. Phys. Lett. 83 (2003), pp. 4157–4159.

[26] V.I. Klimov, C.J. Schwarz, D.W. McBranch, C.A. Leatherdale, and M.G. Bawendi, *Ultrafast dynamics of inter- and intraband transitions in semiconductor nanocrystals: implications for quantum-dot lasers*, Phys. Rev. B. 60 (1999), pp. R2177–R2180.

[27] C.H. Henry and K.K. Nassau, *Lifetimes of bound excitons in CdS*, Phys. Rev. B 1, (1970), pp. 1628–1634.

[28] G.W. p't Hooft, W.A.J.A. van der Poel, and L.W. Molenkamp, *Giant oscillator strength of free excitons in GaAs*, Phys. Rev. B 35 (1987), pp. 8281–8284.

[29] X. Wang, L. Qu, J. Zhang, X. Peng, and M. Xiao, *Surface-related emission in highly luminescent CdSe quantum dots*, Nano Lett. 3 (2003), pp. 1103–1106.

[30] X. Wang, J. Zhang, A. Nazal, M. Darragh, and M. Xiao, *Electronic structure transformation from a quantum-dot to a quantum-wire system: photoluminescence decay and polarization of colloidal CdSe quantum rods*, Appl. Phys. Lett. 81 (2002), pp. 4829–4831.

[31] B.L. Weherenberg, C. Wang, and P. Guyot-Sionnest, *Interband and intraband optical studies of PbSe colloidal quantum dots*, J. Phys. Chem. B 106 (2002), pp. 10634–10640.

[32] M. O'Neil, J. Marhon, and G. McLendon, *Dynamics of electron-hole pair recombination in semiconductor clusters*, J. Phys. Chem. 94 (1990), pp. 4356–4363.

[33] U. Woggon (ed.), *Optical Properties of Semiconductor Quantum Dots*, Springer Tracts in Modern Physics Vol. 136, Springer, Berlin, 1997.

[34] G.A. Woolley, P.C. Biggin, A. Schultz, L. Lien, D.C. Jaikaran, J. Breed, K. Crowhurst, and M.S. Sansom, *Intrinsic rectification of ion flux in alamethicin channels: studies with an alamethicin dimmer*, Bio. Phys. J. 73 (1997), pp. 770–778.

[35] G.S. Harms, G. Orr, M. Montal, B.D. Thrall, S.D. Colson, and H.P. Lu, *Probing conformational changes of gramicidin ion Channels by single-molecule patch-clamp fluorescence microscopy*, Bio. Phys. J. 85 (2003), pp. 1826–1838.

[36] L. Kaestner and I. Bernhardt, *Ion channels in the human red blood cell membrane: their further investigation and physiological relevance*, Bioelectrochemistry 55 (2002), pp. 71–74.

[37] M. Banghart, K. Borges, E. Isacoff, D. Trauner, and R.H. Kramer, *Light-activated ion channels for remote control of neuronal firing*, Nature Neurosci. 7 (2004), pp. 1381–1386.